symmetry

MDPI

Article

Multiconfigurational Dynamical Symmetry Description of ^{40}Ca Spectrum

Chandra Sekhar Panda [1,2], Judit Darai [1], Gábor Riczu [1] and József Cseh [1,*]

[1] HUN-REN Institute for Nuclear Research, P.O. Box 51, 4001 Debrecen, Hungary; chandra.sekhar.panda@atomki.hu (C.S.P.); darai@atomki.hu (J.D.); riczugabor@atomki.hu (G.R.)
[2] Doctoral School of Physics, University of Debrecen, Bem tér 18/B, 4026 Debrecen, Hungary
* Correspondence: cseh@atomki.hu

Abstract

The spectrum of the ^{40}Ca nucleus is known experimentally in different regions of deformation and excitation energy. Its ground state is spherical, and in the low-energy region there are rotational bands corresponding to moderate deformation. Its superdeformed (SD) band is also well-established from gamma-spectroscopy, whereas for hyperdeformation (HD), some indications come from good-resolution heavy-ion resonances. Here we apply multiconfigurational dynamical symmetry (MUSY) for a unified description of this spectrum, including the SD and candidate HD states. This symmetry connects the shell, collective and cluster models; therefore, it provides us with the shape isomers of the nucleus, as well as its spectrum scattered along energy and reaction channels.

Keywords: multiconfigurational dynamical symmetry; clusterization; shape isomers

1. Introduction

The exotic shapes of atomic nuclei attract much attention both from experimental and from theoretical perspectives; see, e.g., refs. [1–6], and the references therein. In light nuclei, several superdeformed bands have been observed experimentally, mainly in multiple gamma-coincidence measurements. In some cases there are indications even of the existence of a hyperdeformed state, though they are obtained not from gamma-spectroscopy, but rather from heavy-ion resonance reactions. Therefore, the available results are not considered clear-cut experimental evidence for the existence of hyperdeformation; nevertheless they are very important observations.

As for the theoretical description or prediction of shape isomers, we are faced with different challenges. We wish to see the spectroscopic characteristics of states, like energy, spin–parity, deformation, electromagnetic transitions, coupling to reaction channels, etc. Furthermore, it is also an interesting and non-trivial question as to whether or not this exotic part of the spectrum, which corresponds to large deformation and high excitation energy, can be understood on the same footing as that applied to the much better-known ground-state region. In many cases the models which are used for the description of the heavy-ion resonances have no connection with standard nuclear structure theory, e.g., to the shell model.

A new symmetry-governed approach, called multiconfigurational dynamical symmetry (MUSY) [7], can address this problem, due to the fact that it gives the common intersection of the shell, collective and cluster models for multi-major-shell problems. This

Academic Editors: Stefano Profumo and Alberto Ruiz-Jimeno

Received: 29 May 2026
Revised: 10 July 2026
Accepted: 12 July 2026
Published: 15 July 2026

approach has been applied for the unified description of the spectrum of the ^{36}Ar nucleus [8], from the ground state up to the resonance spectrum of the heavy-ion reactions, providing a candidate for the hyperdeformed state. It turns out that the gross features of the spectrum can be obtained in a unified way for the first (ground), second (superdeformed) and third (hyperdeformed) minima of the potential energy surface.

For the ^{40}Ca nucleus, the experimental situation is similar: we have a well-established spectrum in the low-energy region, convincing experimental evidence for the superdeformed band, and a remarkable candidate for the hyperdeformed state from heavy-ion reactions. For this reason we address here the question of whether one can obtain a unified description for the gross features of this spectrum. In particular we tend to investigate the prediction of MUSY for the shape isomers and the different parts of the energy spectrum on an equal footing.

In what follows, we first give a short review of the previous investigations both from experimental and from theoretical sides in Section 2. Then in Section 3 the basic features of MUSY are described. Section 4 gives the experimental data, and Section 5 presents the model calculation. Finally a summary is given and conclusions are drawn.

2. Previous Studies

2.1. Experiment

Including the superdeformed (SD) band, four positive-parity bands were reported in the ^{28}Si(^{20}Ne, 2α)^{40}Ca reaction study [9]. Three bands are built on the 0^+ (3.352 MeV), 8^+ (8.103 MeV), and 3^+ (6.03 MeV) bandheads, respectively. The fourth, the SD band, starts at the second excited 0^+ state at 5.211 MeV.

The first three states of the SD band were identified through the ^{36}Ar(^{6}Li, d)^{40}Ca reaction [10]. With the exception of the two highest-spin states, its members were populated in the ^{24}Mg(^{28}Si, 3α)^{40}Ca reaction [11]. All the SD-band states were also observed from the ^{24}Mg(^{24}Mg, 2α)^{40}Ca reaction [12].

A negative-parity band, with its bandhead at the 1^- state (5.902 MeV), was reported in ref. [11]. It has been proposed as the negative-parity partner of the positive-parity band built on the first excited 0^+ state (3.352 MeV) and is referred to as the $K^\pi = 0^-$ band.

The experimental candidates for the hyperdeformed (HD) band were comprehensively compiled by Benjamim et al. [13]. In their work, the authors propose several new HD candidates from their ^{12}C + ^{28}Si scattering experiment and systematically review all previously suggested resonance states from the earlier literature—including both the ^{12}C + ^{28}Si [14,15] and the ^{16}O + ^{24}Mg [16–18] systems—effectively establishing a unified list of HD candidates within the 32.4–52.4 MeV excitation energy range. Out of the proposed candidates for the HD band, four states, 8^+, 10^+, 13^-, and 15^-, at excitation energies of 32.4, 34.0, 35.3, and 37.0 MeV, respectively, have well-established spin and parity. In addition, several candidate states with even and odd angular momenta but uncertain parity have been given. For even angular momenta, these include two $J = 18$ states at 39.4 and 43.6 MeV, three $J = 20$ states at 47.0, 44.0, and 43.8 MeV, and one $J = 26$ state at 52.4 MeV. For odd angular momenta, the candidates include one $J = 13$ state at 34.9 MeV, two $J = 15$ states at 36.6 and 37.8 MeV, one $J = 19$ state at 47.0 MeV, one $J = 21$ state at 44.2 MeV, two $J = 23$ states at 47.0 and 47.4 MeV, and one $J = 25$ state at 50.4 MeV. The states $J = 13$ at 34.9 MeV, $J = 15$ at 36.6 MeV, $J = 18$ at 39.4 and 43.6 MeV, and $J = 20(19)$ at 47.0 MeV are obtained from the ^{12}C + ^{28}Si elastic scattering [14,15], while the other states are resonances observed in the elastic scattering and α-transfer reactions of the ^{16}O + ^{24}Mg system [16–18].

https://doi.org/10.3390/sym18071193

2.2. Theory

The low-lying levels in ^{40}Ca were described in Refs. [19,20] as a mixture of shell-model states and deformed states formed by raising particles from the sd to the fp shell. The first and second excited 0^+ states were suggested to be 4p–4h and 8p–8h excitations, which are the bandheads of the experimentally observed lower-lying positive-parity band and superdeformed (SD) bands [9].

The lower-lying positive-parity band and the only experimentally observed negative-parity band [11] were described within the local potential cluster model [21].

After the experimental confirmation of the SD band, numerous theoretical investigations were carried out using several models. Large-scale shell-model calculations have shown that the SD structure is dominated by multi-particle–multi-hole excitations across the $N = Z = 20$ shell gap, in particular an 8p–8h configuration generating a strongly deformed intrinsic state [22]. In ref. [23] the cranking covariant density functional theory is combined with a shell-model-like approach for the treatment of pairing for the description of the energy spectra and moments of inertia, as well as the transition quadrupole moments of the SD rotational band in ^{40}Ca. With the use of the symmetry-unrestricted cranked Skyrme–Hartree–Fock method, the SD band in ^{40}Ca was found to be extremely soft against both the axially symmetric and asymmetric octupole deformations [24]. In the framework of covariant density functional theory a detailed analysis of the structure of the rotational spectra of ^{40}Ca was presented [25]. The SD states in ^{40}Ca were interpreted as multi-particle–multi-hole (e.g., 8p–8h) excitations within a shell-model-inspired semi-empirical framework [26]. Cranked self-consistent mean-field calculations indicate that signature-dependent triaxiality governs the shape evolution of SD states in ^{40}Ca at high spin [27]. The SD structure of ^{40}Ca has also been described in beyond-mean-field calculations [28]. Alternatively, cluster-based models, such as antisymmetrized molecular dynamics (AMD) and the generator coordinate method (GCM), emphasize the role of cluster correlations in highly deformed states of ^{40}Ca [29,30]. It is found that the band built on the first excited 0^+ state contains an α-cluster component, while the SD band exhibits a ^{12}C + ^{28}Si cluster structure.

Several theoretical studies have explored hyperdeformed (HD) configurations in ^{40}Ca. Fixed-configuration Hartree–Fock calculations predict a stable 12p–12h HD state with $\beta \approx 0.97$ [31], consistent with macroscopic–microscopic results [32]. Cranked Skyrme–Hartree–Fock calculations also identify an HD configuration corresponding to this state [24]. Within a U(3) symmetry framework, two HD candidate configurations were proposed [33], corresponding to the 12p–12h and 16p–16h excitations and associated with the U(3) irreducible representations (irreps) [48,12,12] and [52,12,12], respectively. Covariant density functional theory finds ^{36}Ar and ^{40}Ca to be prime candidates for extremely deformed structures (super-, hyper-, megadeformed) at high spin, with the ^{40}Ca HD state linked to the occupation of the Nilsson orbital 1/2[440] [25]. Energy-density functional studies similarly show HD configurations emerging at high angular momentum when a proton and neutron occupy this orbital, producing $\beta \approx 0.97$ deformation [27]. A shape isomer study [34] based on quadrupole shape stability and self-consistency [35] has found a stable HD state and suggests different binary cluster structures. This state corresponds to the U(3) irrep [56,12,8] of $16\hbar\omega$ excitation.

3. Multiconfigurational Dynamical Symmetry

A unification of the spherical shell model, the collective model and the cluster model was established in 1958 [36–39], when the U(3) dynamical symmetry was found to be the underlying connection among them. This connection initially applied to the single-major-shell problem. Extensive efforts have been made to develop symmetry-governed models for the multi-major-shell problem within the shell model [40,41], collective model [42,43], and cluster model [44,45], and eventually their connection was revealed [7,35]. It was found that the intersection of these fundamental models is once again governed by a generalization of the U(3) dynamical symmetry, called multiconfigurational dynamical symmetry (MUSY).

In the case of the single-shell problem, the spatial part of the shell or quartet configuration is typically described by the algebraic chain of the Elliott model [36,37]:

$$\begin{array}{ccccc} U(3) & \supset & SU(3) & \supset & SO(3), \\ |[n_1, n_2, n_3], & & (\lambda, \mu), & K, & L \;\rangle \end{array} \tag{1}$$

where $\lambda = n_1 - n_2$ and $\mu = n_2 - n_3$, and $K = min\{\lambda, \mu\}, min\{\lambda, \mu\} - 2, ..., 1\ or\ 0$ and $L = K, K+1, ...K + max\{\lambda, \mu\}$, with the exception of $K = 0$, when $L = max\{\lambda, \mu\}$, $max\{\lambda, \mu\} - 2, ..., 1\ or\ 0$.

The spin–isospin part is described by the Wigner $U^{ST}(4)$ group [46]. The U(3) group can be derived from the U(N) group, which shares the same Young pattern as the permutation group, where N denotes the number of orbitals in a single major shell of the harmonic oscillator. Antisymmetrization is satisfied by the associated U(N) and $U^{ST}(4)$ representations, whose Young diagrams are related by reflection, i.e., by interchanging rows and columns [47]. For multi-major-shell problems, this procedure is applied iteratively. Any cluster or collective wave function can be expressed by expanding it in the shell-model U(3) basis.

For a binary cluster configuration, the space part is described by the group chain

$$U_{C_1}(3) \otimes U_{C_2}(3) \otimes U_R(3) \supset U_C(3) \otimes U_R(3) \supset U(3) \supset SU(3) \supset SO(3). \tag{2}$$

Here, C_1 and C_2 denote clusters 1 and 2, $U_C(3)$ represents the combined spatial symmetry of the two clusters, and $U_R(3)$ corresponds to the symmetry of their relative motion. The internal structure of clusters is described by the Elliott model [36,37], while the modified [$U_R(4)$] vibron model [48] accounts for the relative motion of the clusters (R refers to their relative motion). In this case as well, the spin–isospin sector is described by $U^{ST}(4)$, and the antisymmetry condition is fulfilled.

For multi-major-shell problems, a unified classification of the shell, collective, and cluster models is provided by the following group chain:

$$\begin{array}{cccccccc} U_s(3) & \otimes & U_e(3) & \supset & U(3) & \supset\ SU(3) & \supset SO(3) & \\ |[n_1^s, n_2^s, n_3^s], & & [n_1^e, n_2^e, n_3^e], & \rho, & [n_1, n_2, n_3], & (\lambda, \mu), & K, & L \;\rangle, \end{array} \tag{3}$$

where ρ differentiates the repeated occurrences of $[n_1,n_2,n_3]$ arising in the direct product representation ($[n_1^s,n_2^s,n_3^s] \otimes [n_1^e,n_2^e,n_3^e]$). Here, $U_s(3)$ represents the symmetry of the valence shell in both the shell model and the (microscopic) collective model, as well as the spatial symmetry of clusters in the cluster model. On the other hand, $U_e(3)$ corresponds to major-shell excitations, which in the cluster picture are associated with the relative motion between clusters.

MUSY represents a composite symmetry in which each configuration has a standard [U(3)] dynamical symmetry, accompanied by an additional symmetry that connects different configurations [49]. This connecting symmetry corresponds to invariance under transformations in the pseudo-space of particle indices [7]. Through this unifying role, MUSY provides a common framework for describing different configurations, including both shell and cluster structures.

A notable feature of MUSY is its dual symmetry breaking: U(3) and SU(3) symmetries are dynamically broken due to the presence of symmetry-breaking interactions, while the SO(3) symmetry is spontaneously broken in the eigenvalue problem of the intrinsic Hamiltonian [50]. The deformed cluster and shell configurations of the intrinsic states emerge as a consequence of spontaneous symmetry breaking. Such dual symmetry breaking is a common feature of many algebraic structure models with dynamical symmetries [51], including the Elliott model, which serves as their prototype [36,37].

3.1. Shape Isomers

From the Elliott model [36,37], it follows that U(3) serves as a good approximate symmetry in the low-energy region of light nuclei. However, symmetry-breaking interactions—such as spin–orbit coupling and pairing—lead to the breaking of the U(3) symmetry. Remarkably, despite the presence of strong symmetry-breaking effects, a generalized form—known as quasi-dynamical U(3) symmetry—still provides a good description [52]. When the exact symmetry is preserved, however, the quasi-dynamical and exact U(3) symmetries coincide.

The quasi-dynamical generalization provides a method to investigate the stability and self-consistency of the SU(3) symmetry, known as the SCS method [35]. It is an alternative method to the usual energy surface calculation. This method is based on the determination of quasi-dynamical (or effective) SU(3) quantum numbers, which are then translated into quadrupole deformation parameters [53]. The effective SU(3) quantum numbers are derived from the occupancy of the asymptotic Nilsson orbitals [54]. The procedure involves the following steps:

1. First, determine the Nilsson orbitals as functions of the quadrupole deformation parameters by solving the eigenvalue equation of the deformed Hamiltonian with cylindrical symmetry:

$$H = -\frac{\hbar^2}{2M}\Delta + \frac{M}{2}\left[\omega_\perp^2\left(x^2+y^2\right)+\omega_z^2 z^2\right] - c\,(\vec{l}\cdot\vec{s}) - D\,\vec{l}^{\,2}. \tag{4}$$

This Hamiltonian includes the deformed harmonic oscillator potential, along with additional spin–orbit and angular momentum-dependent terms. The elongation parameter ϵ is defined through

$$\omega_z = \omega_0(1-\frac{2}{3}\epsilon), \omega_\perp = \omega_0(1+\frac{1}{3}\epsilon), \epsilon = \frac{\omega_\perp - \omega_z}{\omega_0} \tag{5}$$

The relationship between the elongation parameter ϵ and the conventional quadrupole deformation parameter β is given by $\epsilon \approx 0.95\beta$ [55].

2. Construct the many-particle state by filling the Nilsson orbitals according to the energy-minimum principle and the Pauli exclusion principle.
3. Diagonalize the Hamiltonian corresponding to a triaxial shape, defined by the deformed harmonic oscillator potential

$$V = \frac{M}{2}(\omega_x^2 x^2 + \omega_y^2 y^2 + \omega_z^2 z^2), \tag{6}$$

in cylindrical coordinates. The resulting Nilsson orbitals, corresponding to a given deformation (ϵ,γ), are then expanded in terms of the previously derived asymptotic Nilsson states [56].

4. The effective SU(3) quantum numbers (λ,μ) are obtained from the linear combination of the single-particle orbitals using the relations that are valid in the large-deformation limit.

5. The effective quantum numbers can be converted into the quadrupole deformation parameters (β,γ) [53] using the following relations:

$$\beta^2 = \frac{16\pi}{5N_0^2}(\lambda^2 + \mu^2 + \lambda\mu), \gamma = arctan(\frac{\sqrt{3}\mu}{2\lambda + \mu}). \quad (7)$$

Here, N_0 is the number of oscillator quanta, $N_0 = n_1 + n_2 + n_3 + \frac{3}{2}(A - 1)$. n_1, n_2, and n_3 are the U(3) quantum numbers and A is the mass number of the nucleus.

This procedure makes it possible to investigate the stability and self-consistency of both the effective SU(3) quantum numbers and the deformation parameters.

3.2. Energy

In MUSY, a simple Hamiltonian with dynamical symmetry that is invariant under transformations between different configurations can be applied. It is expressed using the invariants of the second part of the group chain (3); U(3) ⊃ SU(3) ⊃ SO(3):

$$\hat{H} = \hat{C}^{(1)}_{U(3)} + a\hat{C}^{(2)}_{SU(3)} + b\hat{C}^{(3)}_{SU(3)} + d'\hat{C}^{(2)}_{SO(3)}. \quad (8)$$

This Hamiltonian allows the energies to be obtained analytically for various configurations within a unified framework. In the above expression, the effects of shell excitation $U_e(3)$ and internal structure $U_s(3)$ arise only through their coupled [U(3)] representation. The Casimir operator $\hat{C}^{(1)}_{U(3)}$ is associated with the harmonic oscillator Hamiltonian $\{(\hbar\omega)\hat{n}\}$, whereas $\hat{C}^{(2)}_{SU(3)}$ and $\hat{C}^{(2)}_{SO(3)}$ represent the quadrupole–quadrupole and angular momentum interactions, respectively. In the third term $\hat{C}^{(3)}_{SU(3)}$ distinguishes between prolate and oblate nuclear shapes [57]. The eigenvalues of $\hat{C}^{(2)}_{SU(3)}$ and $\hat{C}^{(3)}_{SU(3)}$ corresponding to the SU(3) quantum numbers (λ,μ) are $\lambda^2 + \mu^2 + \lambda\mu + 3(\lambda + \mu)$ and $(\lambda - \mu)(\lambda + 2\mu + 3)(2\lambda + \mu + 3)$, respectively. Furthermore, the expectation value of $\hat{C}^{(2)}_{SO(3)}$ is $L(L + 1)$.

3.3. Electromagnetic Transitions

The reduced transition probability [B(E2)] for the intraband transition from L_i to L_f is given by

$$B(E2, L_i \longrightarrow L_f) = \frac{2L_f + 1}{2L_i + 1}\alpha^2 |\langle(\lambda\mu)KL_i, (11)2||(\lambda\mu)KL_f\rangle|^2 C^{(2)}_{SU(3)} \quad (9)$$

where $\langle(\lambda\mu)KL_i, (11)2||(\lambda\mu)KL_f\rangle$ is an SU(3) ⊃ SO(3) Wigner coefficient [58], and α^2 can be obtained by fitting experimental data. Since the transition operator in Equation (9) is the quadrupole operator, interband transitions vanish. Such transitions can, however, appear due to symmetry-breaking interactions or higher-order transition operators.

4. Experimental Data

Four positive-parity rotational bands were reported in [9]. One of these bands extends from the 0^+ (3.352 MeV) up to the 16^+ (20.578 MeV). In addition, two further positive-parity bands were identified, covering the spin ranges from 8^+ (8.103 MeV) to 15^+ (19.195 MeV) and from 3^+ (6.03 MeV) to 13^+ (16.579 MeV). The SD band, which started from the 0^+ at 5.21 MeV and extended up to the 16^+ at 22.06 MeV, was also identified. A negative-parity band was proposed in Ref. [11].

All the bands mentioned above are reported in the compilation [59,60]. However, the negative-parity band differs between Ref. [11] and the compilation. In the compilation, it spans from (7^-) at 9.033 MeV to (15^-) at 18.215 MeV. In Ref. [11], this band starts with 1^-

at 5.902 MeV and includes two 3^- states at 6.28 MeV and 6.58 MeV, and has an uncertain-parity state with spin 5 at 7.399 MeV below (7^-). However, the spin-5 state with uncertain parity already belongs to the positive-parity band that starts with the 3^+ state at 6.03 MeV, which was proposed earlier [9]. For this reason, we do not consider the spin-5 state to be part of the negative-parity band.

We arranged four positive-parity bands and five negative-parity bands in the low-energy region (0 to 10.04 MeV) using the compilation [59,60]. When at least three experimental states with well-established spin and parity lie approximately on a straight line in an energy versus $J(J+1)$ plot, they are assumed to form a band (Table 1). Although it would have been possible to extend the band assignment to higher excitation energies, the level density in that region is so high that the assignments would not be unambiguous using this method. Furthermore, we refer to these as "assumed bands" because only three E2 transitions are known within these bands, and the corresponding experimental B(E2) values are relatively low. As a result, they are given much less weight in the fitting process. The assumed bands are shown in Figure 1.

Table 1. Parameters of the assumed rotational bands. The parameters of the straight lines $E = E_0 J(J+1) + A$ corresponding to the rotational bands are determined using the least-squares method. The goodness of the fits is characterized by the sums of squared residuals.

Band	2_1^+	2_2^+	0_2^+	2_3^+	2_1^-	2_2^-	3_1^-	1_1^-	1_2^-
E_0	0.101	0.109	0.136	0.105	0.068	0.089	0.073	0.108	0.106
A	4.714	5.721	7.188	6.243	5.695	2.329	6.306	6.798	7.984
$\sum_i (E_i^{exp} - E_i^{fit})^2$	0.111	0.011	0.033	0.005	0.078	0.384	0.018	0.217	0.550

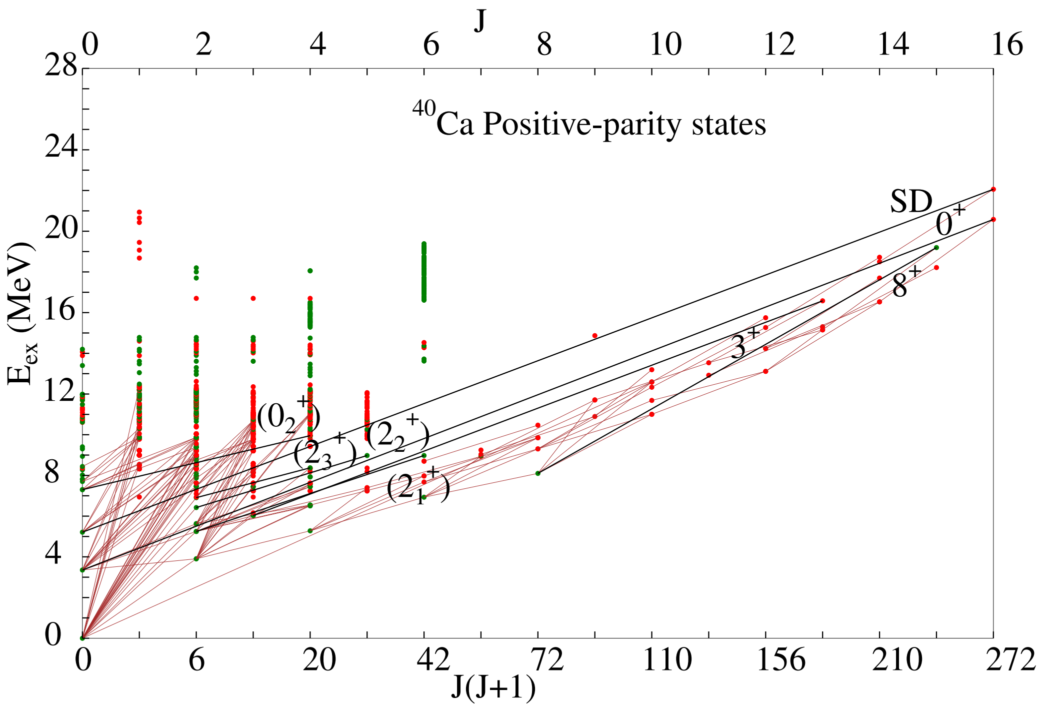

(**a**) Positive-parity states of ^{40}Ca

Figure 1. *Cont.*

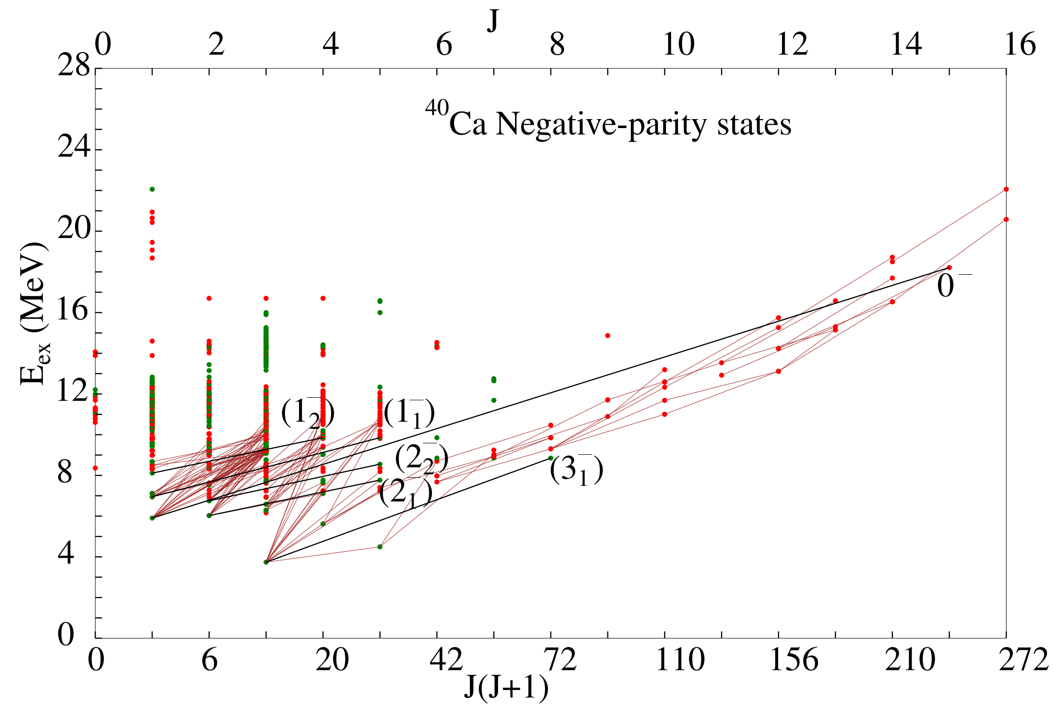

(**b**) Negative-parity states of ^{40}Ca

Figure 1. Energy of positive- and negative-parity states in the ^{40}Ca nucleus as a function of J. The states identified with small green circles correspond to well-established spin–parity assignments, while the small red circles indicate states with uncertain spin–parity assignments. The brown lines connecting the circles represent electromagnetic transitions. All the states shown in the figure are taken from the compilation [59,60]. The black lines indicate rotational bands. In (**a**), the bands built on the 0^+, 8^+, and 3^+ states, as well as the SD band, were previously proposed [9,59,60]. In (**b**), the 0^- band was previously suggested [11,59,60]. The arranged bands are labeled according to the spin–parity (J^π) of their band head, with subscripts used to distinguish between bands with the same bandhead spin–parity.

Eighteen candidate states were proposed for the HD band in Ref. [13]. We classify these states into positive- and negative-parity groups in accordance with our model calculations. As mentioned above, the existence of the HD state has not yet been conclusively established by the available experimental observations. Multi-gamma-coincidence measurements would be highly desirable in this respect. Nevertheless, the heavy-ion resonance data provide a very strong indication. Therefore, when we speak about HD bands in this paper, they should be understood as candidate bands.

5. Model Calculations

5.1. Shape Isomers

The shape isomers were determined using the symmetry-governed stability and self-consistency (SCS) method for the SU(3) symmetry [35], as outlined in the previous section.

The shape isomers can be seen in the $\beta_{in} - \beta_{out}$ plot as horizontal plateaus, as shown in Figure 2. A similar figure appears in [34].

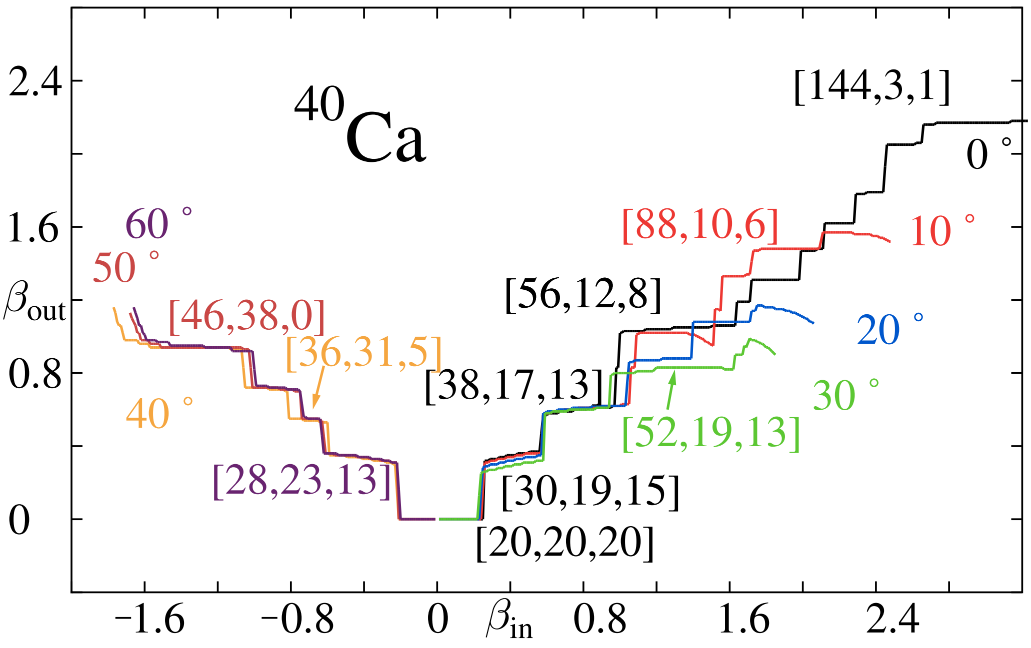

Figure 2. Effective U(3) quantum numbers obtained from the SCS method are used to illustrate the shape isomers of the ^{40}Ca nucleus. β_{in} and β_{out} values are shown on the horizontal and vertical axes, respectively. The γ deformation is indicated in degrees, with 10° increments.

5.2. Model Space

We constructed a no-core shell-model space in which all nucleonic degrees of freedom were included for the application of MUSY. During the construction of this space, spurious center-of-mass excitations were eliminated, and the Pauli exclusion principle was fully respected.

For the construction of the cluster model space, the leading ground state U(3) irreducible representations (irreps) for the internal structure of clusters are considered. These U(3) irreps are: [20,20,12] for ^{36}Ar, [0,0,0] for α, [20,8,8] for prolate and [16,16,4] for oblate shapes of ^{28}Si, $[4,4,0]$ for ^{12}C, $[16,8,4]$ for ^{24}Mg, $[4,4,4]$ for ^{16}O, and $[12,4,4]$ for ^{20}Ne. The relative motion between clusters is constrained by the Wildermuth condition [38], which gives the minimum number of oscillator quanta n_π required for the proper treatment of the Pauli principle. The $U(3)$ representations are then coupled with a wide range of allowed relative motion configurations [61]. Still, some representations are Pauli forbidden. They can be eliminated by matching the cluster U(3) basis with the shell model. For identical clusters ^{20}Ne + ^{20}Ne, an additional requirement must be satisfied: $n_\pi + \lambda_C + \mu_C$ must be even [45]. The quantum numbers (λ_C, μ_C) correspond to the SU(3) configuration resulting from the coupling of U(3) representations of the clusters. The relevant representations for the shell and cluster configurations are listed in Table 2.

When the multiplicity of the relevant U(3) representation in the shell basis is one, the shell and cluster configurations become identical as a consequence of antisymmetrization. An especially interesting case is that of the state $4\hbar\omega$[32,20,12], when each of the five cluster configurations is allowed (Figure 3).

In Figure 3, the shapes of the cluster configurations can be determined using Harvey's prescription [62] and the U(3) selection rule, which describe the structural aspects of nuclear fusion (or fission) in terms of the harmonic oscillator basis. In these configurations, the nuclei are assumed to be in their ground intrinsic states, while collective rotations are allowed.

Table 2. The relevant quartet (shell) and cluster model spaces of the ^{40}Ca nucleus are shown for excitations ranging from 0 to $8\hbar\omega$. Here, n denotes the number of major-shell excitations, while $C^{(2)}$ represents the expectation value of the second-order SU(3) Casimir operator. The states are ordered according to decreasing values of $C^{(2)}$, that is, corresponding to decreasing deformation. The columns labeled C1–C5 give the multiplicities of the SU(3) representations in the cluster model spaces corresponding to the channels: C1 = ^{36}Ar + α, C2 = ^{28}Si$_{\text{pro.}}$ + ^{12}C, C3 = ^{28}Si$_{\text{ob.}}$ + ^{12}C, C4 = ^{24}Mg + ^{16}O, and C5 = ^{20}Ne + ^{20}Ne. The states belonging to a definite U(3) representation are determined as shown by Equation (1).

n	U(3)	SU(3)	$C^{(2)}$	Quartet	C1	C2	C3	C4	C5
0	[20,20,20]	(0,0)	0	1	1		1		
1	[23,20,18]	(3,2)	34	1	1		1		
	[22,20,19]	(2,1)	16	1	1		1		
2	[26,20,16]	(6,4)	106	1	1		1		
	[26,18,18]	(8,0)	88	1			1		
	[24,22,16]	(2,6)	76	1					
	[25,20,17]	(5,3)	73	2	1		2		
	[25,19,18]	(6,1)	64	2			2		
	[24,21,17]	(3,4)	58	2					
	[23,22,17]	(1,5)	49	2					
	[24,20,18]	(4,2)	46	6	1		3		
3	[29,20,14]	(9,6)	216	1	1		1		
	[29,18,16]	(11,2)	186	1			1		
	[27,22,14]	(5,8)	168	1					
	[28,20,15]	(8,5)	168	2	1		2		
	[26,23,14]	(3,9)	153	1					
	[28,19,16]	(9,3)	153	3			3		
4	[32,20,12]	(12,8)	364	1	1	1	1	1	1
	[32,18,14]	(14,4)	322	1			1		1
	[32,16,16]	(16,0)	304	1			1		1
	[31,20,13]	(11,7)	301	2	1		2		
	[30,22,12]	(8,10)	298	1		1			
	[31,19,14]	(12,5)	280	3			3		
5	[34,20,11]	(14,9)	472	1		1	1	1	1
	[34,19,12]	(15,7)	445	2		2	2	1	1
	[33,21,11]	(12,10)	430	2		2			1
	[34,18,13]	(16,5)	424	2			2		1
	[34,17,14]	(17,3)	409	2			2		1
	[33,20,12]	(13,8)	400	6	1	5	5	1	
	[34,16,15]	(18,1)	400	1			1		1
	[32,22,11]	(10,11)	394	3		3			
	[33,19,13]	(14,6)	376	11			4		1
	[31,23,11]	(8,12)	364	4		2			
	[32,21,12]	(11,9)	361	12		4			
	[33,18,14]	(15,4)	358	14			3		
6	[36,20,10]	(16,10)	594	1		1	1	1	1
	[36,19,11]	(17,8)	564	3		3	3	1	1
	[35,21,10]	(14,11)	546	2		2			1
	[36,18,12]	(18,6)	540	6		5	3	1	2
	[36,17,13]	(19,4)	522	4			2		1
	[35,20,11]	(15,9)	513	12		4	5	1	1

Table 2. *Cont.*

n	U(3)	SU(3)	$C^{(2)}$	Quartet	C1	C2	C3	C4	C5
7	[38,20,9]	(18,11)	730	1		1	1	1	1
	[38,19,10]	(19,9)	697	3		3	3	1	2
	[37,21,9]	(16,12)	676	2		2			2
	[38,18,11]	(20,7)	670	7		4	3	1	2
	[38,17,12]	(21,5)	649	10		5	2	1	2
	[37,20,10]	(17,10)	640	13		3	5	1	1
	[38,16,13]	(22,3)	634	8			1		2
8	[40,20,8]	(20,12)	880	1		1	1	1	1
	[40,19,9]	(21,10)	844	2		2	2	1	2
	[39,21,8]	(18,13)	820	1		1			1
	[40,18,10]	(22,8)	814	7		3	3	1	3
	[40,17,11]	(23,6)	790	11		4	2	1	2
	[39,20,9]	(19,11)	781	10		2	5	1	2
	[40,16,12]	(24,4)	772	16		5	1	1	3
	[38,22,8]	(16,14)	766	4		1			2
	[40,15,13]	(25,2)	760	8					1

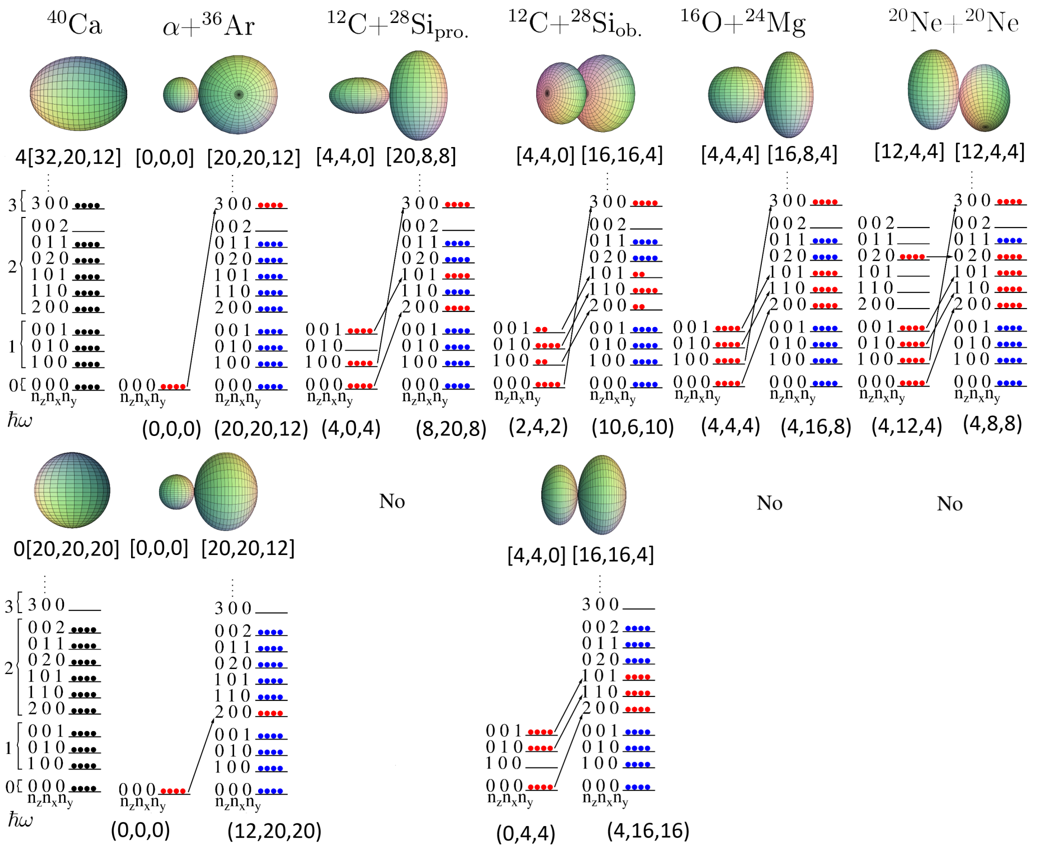

Figure 3. Shapes of the ground state and the most deformed state of $4\hbar\omega$ excitation (i.e., [32,20,12]) of ^{40}Ca are compared with their corresponding binary clusterizations. Harvey's prescription [62] for the amalgamation of the clusters is presented under each configuration. In [ ] the U(3) labels are indicated, while in ( ) the specific basis states are given. The overlap between the cluster- and shell-model wave functions is 100%.

5.3. Spectrum

In order to compute the energy spectrum, we assigned the theoretical bands to the experimental ones. The quantum number of the positive-parity part of the HD band is taken from the SCS calculation [34]. The negative-parity HD band is then assigned the quantum numbers corresponding to configurations closest in deformation to the positive-parity part and possessing appropriate spin–parity content.

The SD band has been interpreted as an 8p–8h configuration on the basis of cranked relativistic mean-field calculations [9]. In Ref. [63], a quasi-dynamical SU(3) quantum number (22,4) in the $8\hbar\omega$ major shell was proposed. We assigned the SU(3) configuration (24,4) from the $8\hbar\omega$ model space to the SD state, which is closest in deformation to (22,4).

The lower-lying positive-parity band was suggested to have a 4p–4h configuration [9,19,20]. This band is described by the most deformed representation of $4\hbar\omega$ model space that has proper spin–parity content. The negative-parity band which was proposed to be the partner of this band [11] has been discussed as the $K^{\pi}=0^-$ band. We interpreted it with the most deformed SU(3) representation (15,4) from the $5\hbar\omega$ model space, which has the appropriate K^{π} and spin–parity content.

The experimentally observed 8^+ and 3^+ bands are interpreted in terms of the SU(3) representations in the model space that are most deformed, with K^{π} values corresponding to the lowest angular momentum of the experimental bands and those that have the correct spin–parity content. Following the same procedure, all arranged bands are described with the most deformed representations in the $1\hbar\omega$, $2\hbar\omega$, and $3\hbar\omega$ model spaces, with each set of SU(3) quantum numbers used only once in the assignment.

We apply the MUSY Hamiltonian, expressed in terms of the invariant operators of the group chain: U(3) ⊃ SU(3) ⊃ SO(3). Then the energy functional is:

$$E = (\hbar\omega)n + a(\lambda^2 + \mu^2 + \lambda\mu + 3(\lambda+\mu)) + b(\lambda-\mu)(\lambda+2\mu+3)(2\lambda+\mu+3) + \frac{d}{2\theta}L(L+1). \tag{10}$$

We note here the simple structure of the applied interactions. In particular, they contain only a major-shell excitation ($\hbar\omega$), a quadrupole interaction (a), a rotational term (d), and a third-order part (b). The first three terms are present even in the Elliott model, while the last one splits the degeneracy of the prolate and oblate shapes.

θ is the moment of inertia and can be calculated either for an ellipsoid with cylindrical symmetry defined by the U(3) quantum numbers, or it can be expressed in terms of the invariant operator; $\theta = a_0 + a_1\hat{C}^{(2)}_{SU(3)}$ [64]. In the present calculation, the former approach is used.

The parameters $\hbar\omega$, a, b, and d are fitted to experimental data. The goodness of the fit is measured by

$$F = \sum_i w(i)\frac{(E_i^{exp} - E_i^{th})^2}{(E_i^{exp})^2}, \tag{11}$$

which is minimized in order to determine the optimal parameters of the Hamiltonian.

While performing the fitting with the experimental states, we follow a weighting strategy that assigns higher priority to experimentally observed and proposed bands, whereas the newly arranged bands are given a lower weight. The complete weighting scheme is as follows: the states belonging to experimentally established bands, including the SD band, and having certain spin–parity, are given as unit weight, whereas states with uncertain spin–parity are assigned a weight of 0.5. For the HD band, states with well-defined spin–parity were weighted by 0.5, while those with uncertain spin–parity were given a weight of 0.25. The exact numbers here are somewhat arbitrary, of course. The basic idea of giving larger preference to the experimentally known states is obviously reasonable, and our experience shows that the actual values of the smaller weights do not considerably influence the results of the fit.

Two different calculations were performed. They differ in the consideration of weights for the arranged bands, as follows:

A. The well-defined spin–parity states of the arranged bands were given a weight of 0.1, while uncertain states were given a weight of 0.05 (Figure 4).
B. All states of the arranged bands were considered with zero weight (i.e., excluded from the fit) (Figure 5).

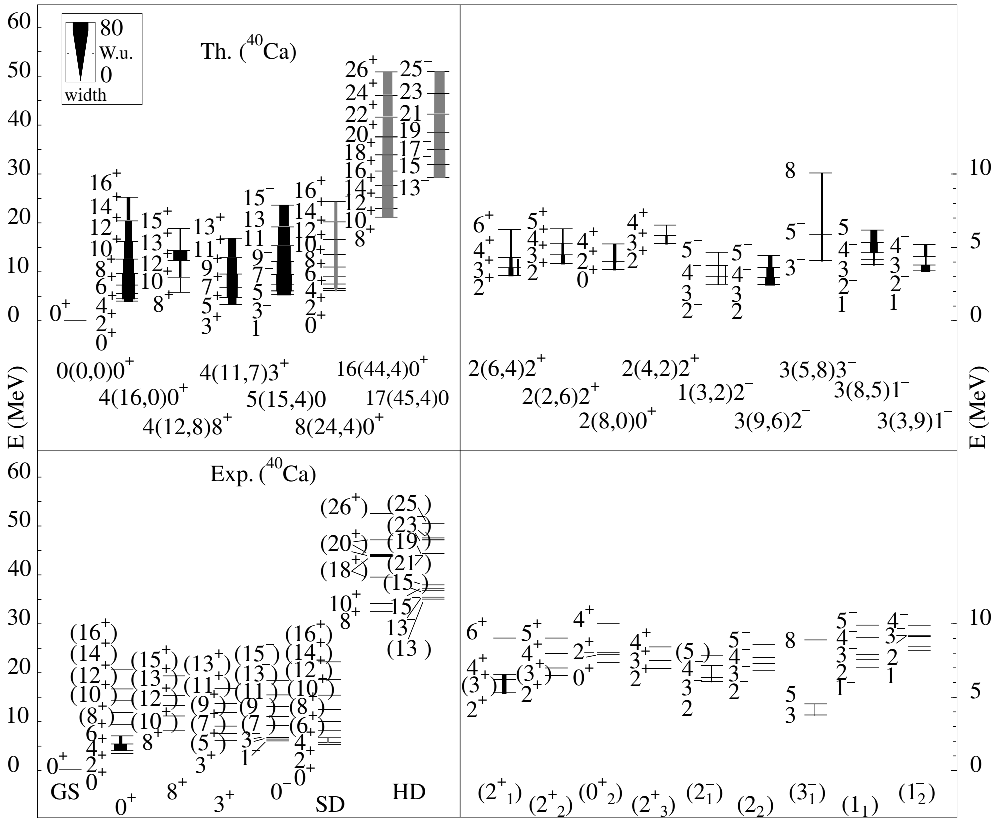

Figure 4. The MUSY spectrum (**top**) is compared with the experimental spectrum of ^{40}Ca (**bottom**). The ground-state, low-lying experimental (and arranged), superdeformed, and hyperdeformed bands are labeled as GS, K$^{\pi}$, SD, and HD, respectively, whereas the theoretical bands are denoted by n(λ,μ)K$^{\pi}$. The bands arranged in this work and the corresponding theoretical spectrum are placed in the right panel of the figure. The widths of the arrows connecting the states are proportional to the corresponding $E2$ transition strengths. For the SD and HD bands, the actual strengths of the gray arrows are ten times larger than those shown. Transitions are displayed from each state to the preceding state with the next lower angular momentum, except for the (2^+_1) $\{4^+ \rightarrow 2^+\}$ and (2^-_1) $\{4^- \rightarrow 2^-\}$ transitions. The corresponding theoretical transitions are plotted slightly to the right of the other theoretical transitions for clarity. This figure shows the spectrum when the well-defined spin–parity states of the arranged bands are assigned a weight of 0.1, while the uncertain states are assigned a weight of 0.05.

The resulting model parameters are listed in Table 3. The change in the parameters of the Hamiltonian and in the quality of the fit indicates the finite accuracy of the predictive power of MUSY. When a larger number of experimental states is included in the fitting procedure (92 instead of 56), the parameters may be modified, which is a natural phenomenon. In this case the difference is not negligible, but it is not drastic either. Therefore, we can say that the extension of the band structure seems to be reasonable.

The intraband transition probability $B(E2)$ (see Equation (9)) was obtained by fitting to the experimental value of the 4^+ (5.278 MeV) $\rightarrow$ 2^+ (3.904 MeV) transition, 67 W.u. ($\alpha^2 = 0.798$). We note here that there are a few experimentally observed interband B(E2) transitions; however, they are considerably weaker than the corresponding intraband transitions. They could be described within the semimicroscopic algebraic cluster model by incorporating the symmetry-breaking terms of the Hamiltonian. In this work we focus on the question of the unified description of different configurations; therefore, we restrict ourselves to symmetric interactions.

Table 3. The parameters of the Hamiltonian and the goodness of the fits, measured by $f = \frac{F}{m}$, where m is the total number of experimental states to be fitted. The two lines represent calculations by including or not including the newly arranged bands (see text for the explanation of A and B). When the newly arranged bands are included, m = 92; when they are excluded, m = 56. For a meaningful comparison between the different calculations, the values of F were recalculated using the same set of weights $w(i)$ when the arranged bands were excluded from the fitting procedure, and the same value m = 92 was used in both cases (f' belongs to these calculations).

	$\hbar\omega$ (MeV)	a (MeV)	b (MeV)	d	f	f'
A.	3.18366	−0.03732	0.00025	1.21304	0.01779	0.01779
B.	2.238319	−0.02379	0.00018	1.18467	0.01562	0.01926

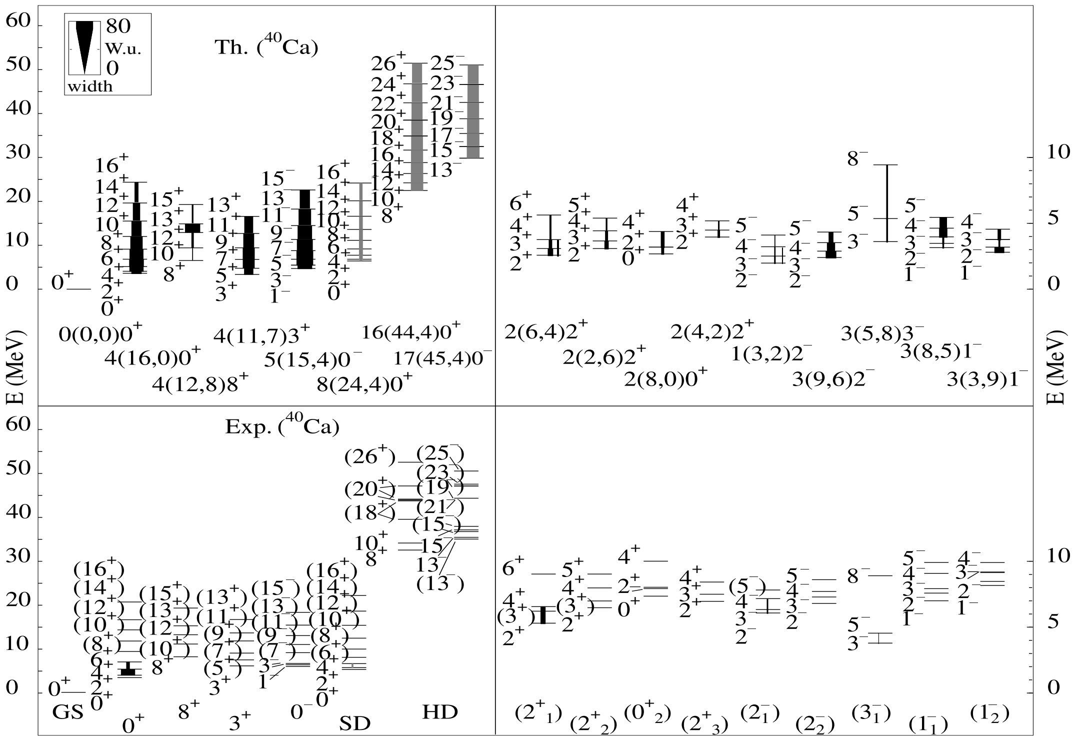

Figure 5. Same as Figure 4, but the states of the arranged bands were given a weight of zero.

6. Summary and Conclusions

In this work we have studied the spectrum of the ^{40}Ca nucleus. In the low-energy region, it has a well-known band structure. Even its superdeformed band is established experimentally, while for its hyperdeformed shape, some indications are available from heavy-ion resonance experiments. We have applied multiconfigurational dynamical symmetry for the unified description of the spectrum. This symmetry provides the common intersection of the shell, collective and cluster models for the general multi-major-shell problem. Therefore, it is able to predict the shape isomers from the behavior of the connecting U(3) symmetry and describe the energy spectrum of different reaction channels in a wide range of energy and deformation values on an equal footing. This treatment combines very large model spaces with a simple dynamically symmetric interaction.

Based on the data of the experimental compilations, we have proposed further candidate bands. They are not considered to be experimentally established. Nevertheless, it is remarkable that (i) their $E - J(J+1)$ plot is linear, and furthermore, (ii) they also seem to fit the unified band structure. In particular, when they were predicted based on the description of better-known bands, the agreement between the experimental and model states was almost as good as that of the fitting procedure (merely 9% difference).

In conclusion we can say that the gross features of the spectrum could be described by MUSY in a unified way to a good approximation. In this respect the situation resembles that of the ^{36}Ar nucleus, where heavy-ion resonances also indicate hyperdeformation. Further experimental investigations along these lines could be very illuminating, especially multiple gamma-coincidence studies which could confirm the existence of HD bands.

Author Contributions: C.S.P.: investigation, visualization, writing; J.D.: investigation, data curation, writing; G.R.: investigation, data curation, validation; J.C.: conceptualization, methodology, writing. All authors have read and agreed to the published version of the manuscript.

Funding: This research received no external funding.

Data Availability Statement: Data are contained within the article.

Acknowledgments: C.S.P. acknowledges the Stipendium Hungaricum Scholarship Programme of the Hungarian Government for the support of his doctoral studies.

Conflicts of Interest: The authors declare no conflicts of interest.

References

1. Leoni, S.; Fornal, B.; Bracco, A.; Tsunoda, Y.; Otsuka, T. Multifaceted character of shape coexistence phenomena in atomic nuclei. *Prog. Part. Nucl. Phys.* **2024**, *139*, 104119. [CrossRef]
2. Leoni, S.; Fornal, B.; Mărginean, N.; Wilson, J.N. Shape isomers: Status and perspectives across the nuclear chart. *Eur. Phys. J. Spec. Top.* **2024**, *233*, 1061–1074. [CrossRef]
3. Lopez-Martens, A.; Lauritsen, T.; Leoni, S.; Døssing, T.; Khoo, T.L.; Siem, S. Population and decay of superdeformed nuclei probed by discrete and quasi-continuum γ-ray spectroscopy. *Prog. Part. Nucl. Phys.* **2016**, *89*, 137–186. [CrossRef]
4. Riley, M. A.; Simpson, J.; Paul, E.S. High resolution gamma-ray spectroscopy and the fascinating angular momentum realm of the atomic nucleus. *Phys. Scr.* **2016**, *91*, 123002. [CrossRef]
5. de Voigt, M.J.A.; Dudek, J.; Szymański, Z. High-spin phenomena in atomic nuclei. *Rev. Mod. Phys.* **1983**, *55*, 949–1046. [CrossRef]
6. Ragnarsson, I.; Bengtsson, T.; Leander, G.; Åberg, S. Nilsson-Strutinsky model of very high spin states. *Nucl. Phys. A* **1980**, *347*, 287–315. [CrossRef]
7. Cseh, J. Microscopic structure and mathematical background of the multiconfigurational dynamical symmetry. *Phys. Rev. C* **2021**, *103*, 064322. [CrossRef]
8. Riczu, G.; Cseh, J. Gross features of the spectrum of the ^{36}Ar nucleus. *Int. J. Mod. Phys. E* **2021**, *30*, 2150034. [CrossRef]
9. Ideguchi, E.; Sarantites, D.G.; Reviol, W.; Afanasjev, A.V.; Devlin, M.; Baktash, C.; Janssens, R.V.F.; Rudolph, D.; Axelsson, A.; Carpenter, M.P.; et al. Superdeformation in the Doubly Magic Nucleus $^{40}_{20}$Ca$_{20}$. *Phys. Rev. Lett.* **2001**, *87*, 222501. [CrossRef] [PubMed]
10. Yamaya, T.; Saitoh, M.; Fujiwara, M.; Itahashi, T.; Katori, K.; Suehiro, T.; Kato, S.; Hatori, S.; Ohkubo, S. Cluster structure in ^{40}Ca via the α-transfer reaction. *Nucl. Phys. A* **1994**, *573*, 154–172. [CrossRef]
11. Torilov, S.; Thummerer, S.; von Oertzen W.; Kokalova, T.; de Angelis, G.; Bohlen, H.G.; Tumino, A.; Axiotis, M.; Farnea E.; Marginean N.; et al. Spectroscopy of ^{40}Ca and negative-parity bands. *Eur. Phys. J. A* **2004**, *19*, 307–317. [CrossRef]
12. Chiara, C.J.; Ideguchi, E.; Devlin, M.; LaFosse, D.R.; Lerma, F.; Reviol, W.; Ryu, S.K.; Sarantites, D.G.; Baktash, C.; Galindo-Uribarri A.; et al. Transition quadrupole moments in the superdeformed band of ^{40}Ca. *Phys. Rev. C* **2003**, *67*, 041303(R). [CrossRef]
13. Benjamim, E.A.; Lépine-Szily, A.; Oliveira, J.M., Jr.; Villari, A.C.C.; Lichtenthäler, R.; Chamon, L.C.; Guimarães, V.; Sciani, W.; Kuramoto, R.Y.R.; Alcantara, J.A.; et al. Cluster structures observed in ^{40}Ca from ^{12}C + ^{28}Si scattering. *J. Phys. Conf. Ser.* **2013**, *436*, 012015. [CrossRef]
14. Ost, R.; Clover, M.R.; DeVries, R.M.; Fulton, B.R.; Gove, H.E.; Rust, N.J. Resonant heavy-ion elastic scattering from s-d shell nuclei. *Phys. Rev. C* **1979**, *19*, 740–746. [CrossRef]
15. Clover, M.R.; DeVries, R.M.; Ost, R.; Rust, N.J.A.; Cherry, R.N., Jr.; Gove, H.E. Resonant Backward-Angle Heavy-Ion Elastic Scattering. *Phys. Rev. Lett.* **1978**, *40*, 1008–1010. [CrossRef]

16. Paul, M.; Sanders, S.J.; Cseh, J.; Geesaman, D.F.; Henning, W.; Kovar, D.G.; Olmer, C.; Schiffer, J.P. Resonant Effects in the Reaction ^{24}Mg(^{16}O, ^{12}C) ^{28}Si. *Phys. Rev. Lett.* **1978**, *40*, 1310–1312. [CrossRef]
17. Lee, S.M.; Adloff, J.C.; Chevallier, P.; Disdier, D.; Bauch, V.; Scheibling, F. Entrance-Channel Resonance Effects in the ^{24}Mg + ^{16}O Reaction. *Phys. Rev. Lett.* **1979**, *42*, 429–432. [CrossRef]
18. Sanders, S.J.; Paul, M.; Cseh, J.; Geesaman, D.F.; Henning, W.; Kovar, D.G.; Kozub, R.; Olmer, C.; Schiffer, J.P. Resonant behavior of the ^{24}Mg(^{16}O, ^{12}C) ^{28}Si reaction. *Phys. Rev. C* **1980**, *21*, 1810–1818. [CrossRef]
19. Gerace, W.J.; Green, A.M. The effect of deformed states in the Ca isotopes. *Nucl. Phys. A* **1967**, *93*, 110–132. [CrossRef]
20. Gerace, W.J.; Green, A.M. K-Band mixing and 8p–8h states in ^{40}Ca. *Nucl. Phys. A* **1969**, *123*, 241–249. [CrossRef]
21. Torilov, S.Y. Energy splitting of the states in the rotational bands in ^{40}Ca. *Eur. Phys. J. A* **2014**, *50*, 3. [CrossRef]
22. Caurier, E.; Menéndez, J.; Nowacki, F.; Poves, A. Coexistence of spherical states with deformed and superdeformed bands in doubly magic ^{40}Ca: A shell-model challenge. *Phys. Rev. C* **2007**, *75*, 054317. Erratum in *Phys. Rev. C* **2007**, *76*, 049901. [CrossRef]
23. Wang, F.; Shi, Z.; Xia, X.W. Description of the superdeformed rotational band in ^{40}Ca with a shell-model-like approach. *Phys. Rev. C* **2020**, *102*, 014321. [CrossRef]
24. Inakura, T.; Mizutori, S.; Yamagami, M.; Matsuyanagi, K. Cranked Skyrme–Hartree–Fock calculation for superdeformed and hyperdeformed rotational bands in N = Z nuclei from ^{32}S to ^{48}Cr. *Nucl. Phys. A* **2002**, *710*, 261–278. [CrossRef]
25. Ray, D.; Afanasjev, A.V. From superdeformation to extreme deformation and clusterization in the N $\approx$ Z nuclei of the A $\approx$ 40 mass region. *Phys. Rev. C* **2016**, *94*, 014310. [CrossRef]
26. Röpke, H. Systematics of deformed states around doubly-magic ^{40}Ca. *Eur. Phys. J. A* **2004**, *22*, 213–230. [CrossRef]
27. Sakai, S.; Yoshida, K.; Matsuo, M. Signature-dependent triaxiality for shape evolution from superdeformation in rapidly rotating ^{40}Ca and ^{41}Ca. *Prog. Theor. Exp. Phys.* **2020**, 063D02. [CrossRef]
28. Bender, M.; Flocard, H.; Heenen, P.-H. Beyond-mean-field-model analysis of low-spin normal-deformed and superdeformed collective states of ^{32}S, ^{36}Ar, ^{38}Ar, and ^{40}Ca. *Phys. Rev. C* **2003**, *68*, 044321. [CrossRef]
29. Kanada-En'yo, Y.; Kimura, M. Superdeformation and clustering in ^{40}Ca studied with antisymmetrized molecular dynamics. *Phys. Rev. C* **2005**, *72*, 064322. [CrossRef]
30. Taniguchi, Y.; Kimura, M.; Kanada-En'yo, Y.; Horiuchi, H. Clustering and triaxial deformations of ^{40}Ca. *Phys. Rev. C* **2007**, *76*, 044317. [CrossRef]
31. Zheng, D.C.; Zamick, L.; Berdichevsky, D. Superdeformed many-particle–many-hole states in N = Z nuclei: Beyond the 8p—8h state in ^{40}Ca. *Phys. Rev. C* **1990**, *42*, 1004–1008. [CrossRef] [PubMed]
32. Leander, G.; Larsson, S.E. Potential-energy surfaces for the doubly even N = Z nuclei. *Nucl. Phys. A* **1975**, *239*, 93–113. [CrossRef]
33. Cseh, J.; Darai, J.; Antonenko, N.V.; Algora, A.; Hess, P.O.; Jolos, R.V.; Scheid, W. Deformation inside and outside the nuclear molecules. *Rev. Mex. Física S* **2006**, *52*, 11–16.
34. Dang, P.; Riczu, G.; Cseh, J. Shape isomers of α-like nuclei in terms of the multiconfigurational dynamical symmetry. *Phys. Rev. C* **2023**, *107*, 044315. [CrossRef]
35. Cseh, J.; Riczu, G.; Darai, J. Shape isomers of light nuclei from the stability and consistency of the SU(3) symmetry. *Phys. Lett. B* **2019**, *795*, 160–164. [CrossRef]
36. Elliott, J.P. Collective Motion in the Nuclear Shell Model. I. Classification Schemes for States of Mixed Configurations. *Proc. R. Soc. Lond. A* **1958**, *245*, 128–145. [CrossRef]
37. Elliot, J.P. Collective Motion in the Nuclear Shell Model. II. The Introduction of Intrinsic Wave-Functions. *Proc. R. Soc. Lond. A* **1958**, *245*, 562–581. [CrossRef]
38. Wildermuth, K.; Kanellopoulos, T. The "clustermodel" of the atomic nuclei. *Nucl. Phys.* **1958**, *7*, 150–162. [CrossRef]
39. Bayman, B.F.; Bohr, A. On the connection between the cluster model and the SU_3 coupling scheme for particles in a harmonic oscillator potential. *Nucl. Phys.* **1958**, *9*, 596–599. [CrossRef]
40. Rosensteel, G.; Rowe, D. Nuclear Sp(3,R) Model. *Phys. Rev. Lett.* **1977**, *38*, 10–14. [CrossRef]
41. Rosensteel, G.; Rowe, D. On the algebraic formulation of collective models III. The symplectic shell model of collective motion. *Ann. Phys.* **1980**, *126*, 343–370. [CrossRef]
42. Rowe, D.; Rosensteel, G. Rotational bands in the U(3)-boson model. *Phys. Rev. C* **1982**, *25*, 3236(R). [CrossRef]
43. Castaños, O.; Draayer, J.P. Contracted symplectic model with ds-shell applications. *Nucl. Phys. A* **1989**, *491*, 349–372. [CrossRef]
44. Cseh, J. Semimicroscopic algebraic description of nuclear cluster states. Vibron model coupled to the SU(3) shell model. *Phys. Lett. B* **1992**, *281*, 173–177. [CrossRef]
45. Cseh J.; Lévai, G. Semimicroscopic Algebraic Cluster Model of Light Nuclei. I. Two-Cluster-Systems with Spin-Isospin-Free Interactions. *Ann. Phys.* **1994**, *230*, 165–200. [CrossRef]
46. Wigner, E.P. On the Consequences of the Symmetry of the Nuclear Hamiltonian on the Spectroscopy of Nuclei. *Phys. Rev.* **1937**, *51*, 106–119. [CrossRef]
47. Elliott, J.P.; Dawber, P.G. *Symmetry in Physics (Volume 1: Principles and Simple Applications)*; Macmillan Press Ltd.: London, UK, 1979.

48. Iachello, F.; Levine, R.D. Algebraic approach to molecular rotation vibration spectra. I. Diatomic molecules. *J. Chem. Phys.* **1982**, *77*, 3046–3055. [CrossRef]
49. Cseh, J. On the Logical Structure of Composite Symmetries in Atomic Nuclei. *Symmetry* **2023**, *15*, 371. [CrossRef]
50. Cseh, J. Spontaneous symmetry-breaking in Elliott-type models and the nuclear deformation. *Phys. Lett. B* **2019**, *793*, 59–64. [CrossRef]
51. Cseh, J. Dual breaking of symmetries in algebraic models. *Eur. Phys. J. Spec. Top.* **2020**, *229*, 2543–2554. [CrossRef]
52. Rowe, D.J. Embedded Representation and Quasi-Dynmical Symmetry. In *Computational and Group-Theoretical Methods in Nuclear Physics, Proceedings of the Symposium in Honor of Jerry P Draayer's 60th Birthday, Playa del Carmen, Mexico, 18–21 February 2003*; Escher, J., Castanos, O., Hirsch, J.G., Pittel, S., Stoitcheva, G., Eds.; World Scientific: Singapore, 2004; pp. 165–173.
53. Rowe, D.J. Microscopic theory of the nuclear collective model. *Rep. Prog. Phys.* **1985**, *48*, 1419–1480. [CrossRef]
54. Jarrio, M.; Wood, J.; Rowe, D.J. The SU(3) structure of rotational states in heavy deformed nuclei. *Nucl. Phys. A* **1991**, *528*, 409–435. [CrossRef]
55. Nilsson, S.G.; Ragnarsson, I. *Shapes and Shells in Nuclear Structure*; Cambridge University Press: Cambridge, UK, 1995.
56. Hess, P.; Algora, A.; Hunyadi, M.; Cseh, J. Configuration-mixed effective SU(3) symmetries. *Eur. Phys. J. A* **2002**, *15*, 449–454. [CrossRef]
57. Cseh, J.; Riczu, G. Quartet excitations and cluster spectra in light nuclei. *Phys. Lett. B* **2016**, *757*, 312–316. [CrossRef]
58. Akiyama, Y.; Draayer, J.P. A user's guide to for tran programs for Wigner and Racah coefficients of SU_3. *Comput. Phys. Commun.* **1973**, *5*, 405–415. [CrossRef]
59. Chen, J. Nuclear Data Sheets for A=40. *Nucl. Data Sheets* **2017**, *140*, 1–376. [CrossRef]
60. National Nuclear Data Center (NNDC). NuDat 3.0. Available online: https://www.nndc.bnl.gov/nudat3/getdataset.jsp?nucleus=40Ca&unc=NDS (accessed on 1 June 2025).
61. Lévai, G.; Cseh, J.; Scheid, W. Semimicroscopic algebraic study of the α-cluster states of the ^{18}O nucleus. *Phys. Rev. C* **1992**, *46*, 548–557. [CrossRef] [PubMed]
62. Harvey, M. *Proceedings of the Second International Conference on Clustering Phenomena in Nuclei, College Park, Maryland, 21–25 April 1975*; USDERA Report ORO-529 4856-26; University of Maryland: College Park, MD, USA, 1975; p. 549.
63. Riczu, G.; Darai, J.; Cseh, J. Superdeformation and dynamical symmetry. *Phys. Scr.* **2024**, *99*, 045306. [CrossRef]
64. Cseh, J.; Riczu, G. Moment of Inertia and Dynamical Symmetry. *Symmetry* **2023**, *15*, 2116. [CrossRef]